

Effect of solid-state synthesized alumina properties on the structure and catalytic performance of NiMo catalyst in hydrodesulfurization

Min Zhang, Tao Yang, Ruiyu Zhao*, Chenguang Liu

State Key Laboratory of Heavy Oil Processing, Key Laboratory of Catalysis, China National Petroleum Corporation (CNPC), China University of Petroleum (East China), Qingdao 266580, PR China

ARTICLE INFO

Article history:

Received 3 May 2013

Received in revised form 4 September 2013

Accepted 5 September 2013

Available online 14 September 2013

Keywords:

AACH

Hydrodesulfurization catalyst

Structural features

Physicochemical properties

Catalytic performance

ABSTRACT

In this paper, a precursor ammonium aluminum carbonate hydroxide (AACH) was synthesized by a low-temperature solid-state reaction, then alumina labeled as Al_2O_3 -AC was obtained by the calcination of AACH, and finally, catalyst labeled as NiMo/ Al_2O_3 -AC supported on Al_2O_3 -AC was prepared using the method of incipient wetness impregnation. The properties of both support and catalyst were investigated by a series of characterization methods. The results indicated that Al_2O_3 -AC had unique bimodal porous structure, high acid content and five-fold coordinated aluminum (AlO_5) on the surface. Moreover, NiMo/ Al_2O_3 -AC exhibited uniform dispersion of active components, higher Brønsted acid sites concentration and weaker metal-support interaction. Encouraged by those excellent properties of Al_2O_3 -AC and NiMo/ Al_2O_3 -AC, the catalyst NiMo/ Al_2O_3 -AC was evaluated in the hydrodesulfurization (HDS) of dibenzothiophene (DBT), showing high conversion ratio of DBT.

© 2013 Elsevier B.V. All rights reserved.

1. Introduction

It is well documented that the support can significantly influence the properties and performance of hydrodesulfurization (HDS) catalysts, such as the reducibility, sulfidability, structure and dispersion of the deposited metal oxides, as well as the morphology of the sulfided active phases [1]. Vissers et al. [2] reported that carbon-supported CoMoS were more weakly bound to the support than metal oxide supports, this weak interaction increased the reducibility of sulfide phase, which further led to a higher catalytic activity. Liu et al. [3] synthesized a novel alumina with bimodal mesoporous structure, which contributed to high crystal phase dispersion and enhanced the catalytic properties for DBT conversion. In all, the support may accelerate or slow down the sulfidation process and determine the final dispersion state [2,4]. Therefore, the choice of proper supports is very important, because they are closely related to the progress concerning catalytic performance of HDS catalysts.

γ - Al_2O_3 owing to its low cost, high specific area, good thermal stability, tunable acidity and its interaction with deposited transition metals, has been widely used as catalyst supports [5–9].

Traditionally, γ - Al_2O_3 is produced by thermal dehydration reaction of well-defined boehmite [9,10]. Compared to the synthesis of boehmite, the preparation of AACH by a low temperature solid-state reaction is relatively simple, efficient and cost-saving [11–15]. Our group [16] has reported the detailed properties of alumina prepared by thermal decomposition of AACH precursor using low-temperature solid-state reaction, but some important aspects were not reported, such as the surface acidity of alumina and reducibility of deposited metal oxides. As is well-known, those aspects have close relationship to the interactions between active metal and alumina surface, which directly influence the dispersion and composition of active phase, as well as the catalytic performance thereof.

In the present work, we try to get a deep insight into the effect of solid-state synthesized alumina properties on the structure and catalytic performance of NiMo catalyst in HDS. In contrast, alumina labeled as Al_2O_3 -SB and catalyst labeled as NiMo/ Al_2O_3 -SB were also prepared using pseudo-boehmite as precursor. The textual and surface properties of alumina were characterized with scanning electron microscopy, nitrogen adsorption, Fourier transform infrared, temperature-programmed desorption of ammonia and ^{27}Al MAS NMR. The structural properties of the catalysts were tested by X-ray powder diffraction, Fourier transform infrared, H_2 -temperature programmed reduction, transmission electron microscopy, and their catalytic performance was tested in the HDS of DBT.

* Corresponding author. Tel.: +86 532 86983057; fax: +86 532 86981787.

E-mail addresses: zgsydzxm@163.com (M. Zhang), yang_tao9364@126.com (T. Yang), zhaory@upc.edu.cn (R. Zhao), cgliu@upc.edu.cn (C. Liu).



2. Experimental

2.1. Materials and preparation

Pseudo-boehmite (SB) powder was industrial grade reagent produced by Germany Condea Co., and the other chemicals were of analytical grade, purchased from National Medicine Group Chemical Reagent Co., Ltd. The precursor AACH was synthesized according to the reference [16]. In a typical experiment, 0.16 ml of poly-glycol (PEG)-400 was mixed with 15.80 g of NH_4HCO_3 powder in agate mortar and ground sufficiently. The powder of $\text{Al}(\text{NO}_3)_3 \cdot 9\text{H}_2\text{O}$ (molar ratio of $\text{NH}_4\text{HCO}_3/\text{Al} = 4/1$) was added into mixture and ground at room temperature for 20 min, then transferred to a Teflon-lined stainless-steel autoclave and placed in an oven at 100 °C. No solvent was used during the process. After aging for about 12 h, the solid precipitation was filtered off, washed with deionized water and anhydrous ethanol to remove the impurity ions, then dried at 100 °C in a vacuum oven for 2 h.

Afterwards, 50 g of as-obtained AACH and SB were extruded. The extrudates were cooled naturally, dried in air at 120 °C for 6 h, and then calcined in muffle furnace at 500 °C for 4 h at 2 °C/min heating rate. The as-obtained $\gamma\text{-Al}_2\text{O}_3$ samples were labeled as $\text{Al}_2\text{O}_3\text{-AC}$ and $\text{Al}_2\text{O}_3\text{-SB}$, respectively. Using $\text{Al}_2\text{O}_3\text{-AC}$ and $\text{Al}_2\text{O}_3\text{-SB}$ as supports, the Ni and NiMo supported catalysts were prepared by incipient impregnation with solution of nickel nitrate ($\text{Ni}(\text{NO}_3)_2 \cdot 6\text{H}_2\text{O}$) and mixed solution of ammonium heptamolybdate ($(\text{NH}_4)_6\text{Mo}_7\text{O}_{24} \cdot 4\text{H}_2\text{O}$) and nickel nitrate ($\text{Ni}(\text{NO}_3)_2 \cdot 6\text{H}_2\text{O}$), respectively. Then the impregnated materials were dried in air at 120 °C for 6 h, and further calcined in muffle furnace at 500 °C for 4 h at 3 °C/min heating rate. The as-prepared catalysts were labeled as $\text{Ni}/\text{Al}_2\text{O}_3\text{-AC}$, $\text{Ni}/\text{Al}_2\text{O}_3\text{-SB}$, $\text{NiMo}/\text{Al}_2\text{O}_3\text{-AC}$ and $\text{NiMo}/\text{Al}_2\text{O}_3\text{-SB}$, respectively.

2.2. Characterization

2.2.1. X-ray powder diffraction

The X-ray powder diffraction (XRD) patterns of the samples were recorded at room temperature by a Panalytical X'Pert Pro MPD diffractometer (the Netherlands) using Cu K_α radiation at a scan rate (2θ) of 5°/min. The accelerating voltage and applied current were 40 kV and 40 mA, respectively.

2.2.2. Electron microscopy

The morphology images of as-prepared samples were obtained by an S-4800 field emission scanning electron microscopy (FE-SEM, Hitachi, Japan) with an acceleration voltage of 1.5 kV. The high resolution transmission electron microscopy (HRTEM) images of the samples were taken using a JEOL JEM-2100 UHR microscope. The catalysts were firstly ground and then suspended in alcohol by an ultrasonic bath, and finally they were placed in a Cu cellulose coated grille.

2.2.3. Textural analysis

The specific surface area and pore size distributions were obtained from nitrogen adsorption-desorption isotherms measured on a Micromeritics TRISTAR 3020 adsorption analyzer (USA) at -196 °C. All as-prepared samples were degassed at 140 °C in vacuum for 6 h prior to adsorption measurements. The surface area was calculated by the Brunauer–Emmett–Teller (BET) method, and the pore size distributions were determined by the Barrett–Joyner–Halenda (BJH) method from the desorption branch of the isotherms.

2.2.4. Fourier transform infrared (FTIR) spectroscopy

The types of surface acid sites on calcined samples were determined through FTIR pyridine adsorption technique. Measurements

were performed on a Newus Fourier transform infrared spectrometer (Nicolet, USA). Prior to measurement, the samples were degassed in air at 350 °C for 3 h, cooled down and then adsorbed in the saturated pyridine atmosphere at room temperature for 2 h. After adsorption, the infrared spectrum was recorded with the sample temperature fixed at 100 °C while outgassing.

2.2.5. ^{27}Al MAS NMR measurements

One-pulse solid-state ^{27}Al MAS NMR spectra were acquired at a frequency of 104.3 MHz on a Bruker Avance 300 spectrometer (Switzerland) by using a 5-mm MAS probe with a spinning rate of 10 kHz. Short single pulses ($\pi/18$) were used with a reprocess time of 1.0 s. The ^{27}Al chemical shifts were referenced to 1 N aqueous solution of AlCl_3 .

2.2.6. Temperature-programmed reduction and desorption of ammonia

Temperature-programmed reduction (TPR) was conducted with a Quantachrome CHEMBET-3000 instrument. The sample (0.1 g) was charged in a loop and heated up to 150 °C at the rate of 10 °C/min, held at 150 °C for 1 h and cooled to room temperature in He flow to remove the adsorbed materials. The treated sample was heated to 700 °C at a rate of 10 °C/min in a mixture of 10 vol% H_2/Ar (100 ml/min). Temperature-programmed desorption of ammonia ($\text{NH}_3\text{-TPD}$) was also conducted to determine the total acidity of supports. The sample (0.1 g) was charged in the loop and heated up to 500 °C at the rate of 10 °C/min, held at 500 °C for 30 min to ensure complete removal of impurities. Then the sample was cooled down to 100 °C and saturated with ammonia and was flushed by He flow for 1 h to remove physically adsorbed ammonia, afterwards the sample was heated to 500 °C at a heating rate of 10 °C/min in He flow (30 ml/min). TCD detector was used to monitor the desorbed ammonia.

2.3. Catalytic performance test

Catalytic activity measurements were carried out in a high-pressure continuous-flow micro-reactor. Generally, 5 ml of the catalyst extrudates were loaded in the reactor. Prior to reaction, the catalysts were sulfided at 300 °C and under 2.0 MPa H_2 pressure for 6 h with a liquid stream containing 3 wt% CS_2 in cyclohexane solution, liquid hour space velocity (LHSV) 2.0 h⁻¹, and $\text{H}_2/\text{feed} = 300/1$. The model compound (2.06 wt% dibenzothiophene dissolved in toluene) was then pumped into reactor. The reaction was carried out at a temperature 240 °C under the conditions of H_2 pressure 2.0 MPa, $\text{H}_2/\text{feed} = 300/1$, and LHSV 4.0 h⁻¹. The liquid product was analyzed at Varian 3800 gas chromatograph equipped with CP-5 capillary column and flame ionization detector.

3. Results and discussion

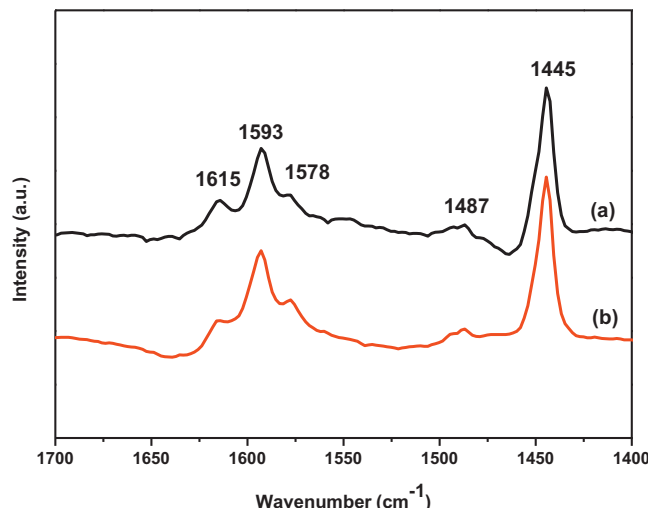
3.1. Acidity of supports

In order to detect the surface acidity, pyridine adsorption/desorption experiments have been carried out on $\text{Al}_2\text{O}_3\text{-AC}$ and $\text{Al}_2\text{O}_3\text{-SB}$ supports, and the results are shown in Fig. 1. The IR spectra display bands ranging from 1445 cm⁻¹ to 1650 cm⁻¹. The band at 1615 cm⁻¹ is assigned to pyridine coordinately bonded to moderate Lewis acid sites of the alumina support and the band at 1593 cm⁻¹ is due to pyridine adsorbed on weak Lewis acid sites. The band at 1578 cm⁻¹ is also attributed to pyridine coordinated to Lewis acid sites [17–19]. From the results, it can be found that there are only weak and moderate Lewis acid sites existing on the surface of both $\text{Al}_2\text{O}_3\text{-SB}$ and $\text{Al}_2\text{O}_3\text{-AC}$. Besides, no bands around 1540 cm⁻¹ are detected, indicating the absence of Brønsted acid

Table 1

Acid content distribution of supports and catalysts.

Supports	Weak acid (<300 °C) (mmol/g)	Moderate acid (300–450 °C) (mmol/g)	Strong acid (450–500 °C) (mmol/g)	Total acidity (mmol/g)
Al ₂ O ₃ -AC	0.274	0.136	0	0.410
Al ₂ O ₃ -SB	0.222	0.128	0	0.350
NiMo/Al ₂ O ₃ -AC	0.281	0.264	0	0.545
NiMo/Al ₂ O ₃ -SB	0.248	0.169	0	0.417

**Fig. 1.** IR spectra of pyridine adsorbed on support (a) Al₂O₃-AC and (b) Al₂O₃-SB.

sites on the surface of those two supports. The acidity of alumina is originated from the unsaturated aluminum coordination and surface hydroxyl groups [20,21]. Liu [22] found that various OH groups were adjacent to different Lewis acid sites, which could determine the interactions between pyridine and OH groups. The author also assigned these different types of Lewis acid sites to several possible Al³⁺ coordination configurations.

Table 1 shows the NH₃-TPD data of Al₂O₃-AC and Al₂O₃-SB samples. It is generally accepted that acid sites are classified into three types: weak ($T_{des} < 300$ °C), medium (300 °C $< T_{des} < 450$ °C) and strong ($T_{des} > 450$ °C) [23]. According to the data of acidic properties in **Table 1**, no strong acid sites are detected on both Al₂O₃-SB and Al₂O₃-AC, which is in accordance with the FTIR results.

Table 2Data of textural properties of Al₂O₃-SB and Al₂O₃-AC.

Supports	BET specific surface area (m ² /g)	Pore volume (ml/g)	Average pore diameter (nm)
Al ₂ O ₃ -AC	335	1.3	12.6
Al ₂ O ₃ -SB	283	0.6	8.0

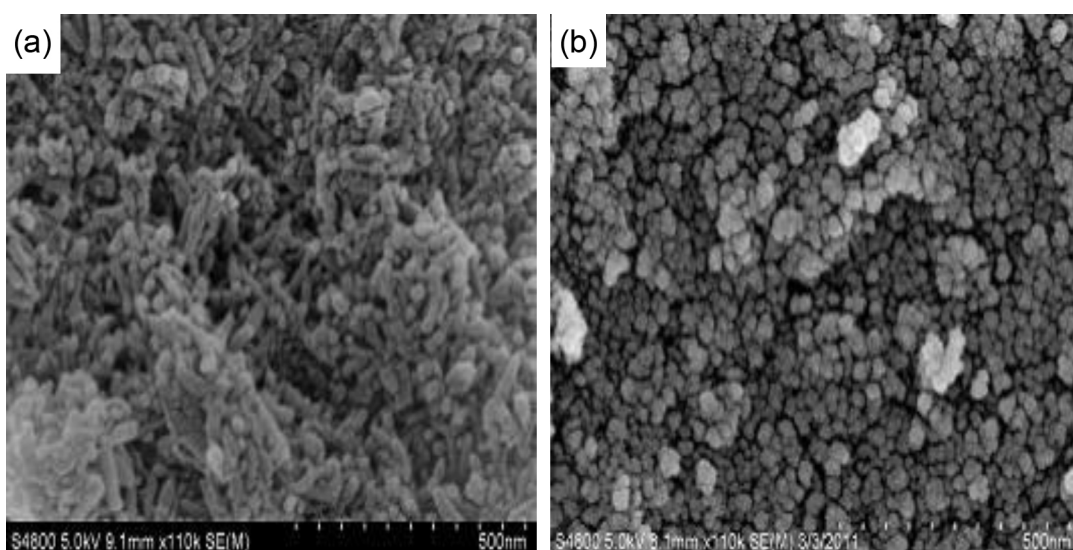
Furthermore, Al₂O₃-AC has more weak and medium strong acid sites than Al₂O₃-SB, which may influence the activity of the catalyst in the HDS reaction. The correlation between the acidity nature and HDS activity has been reported in relevant references [24–26].

3.2. Morphology of the precursors

Fig. 2 shows SEM image of AACH and SB. Compared to the morphology of SB sample with spherical particles packed closely, the AACH sample mainly consists of uniform nanorods about 30–50 nm. The difference in morphology of precursors is associated with the crystal orientation and different planes of crystal particles. Various proportions of different crystallographic surfaces can lead to diverse acid properties [17], which further demonstrate the results of NH₃-TPD.

3.3. Textural property of supports

The specific surface area, pore volume, and average pore diameter of Al₂O₃-AC and Al₂O₃-SB samples are listed in **Table 2**. Apparently, compared to Al₂O₃-SB, Al₂O₃-AC has higher specific surface area and larger pore volume. **Fig. 3** shows the nitrogen adsorption–desorption isotherms and pore size distributions of Al₂O₃-AC and Al₂O₃-SB. The isotherms for those two samples are of type IV, suggesting the presence of mesopores. Besides, Al₂O₃-AC shows higher saturated adsorption amount of nitrogen than that of

**Fig. 2.** SEM images of (a) AACH and (b) SB.

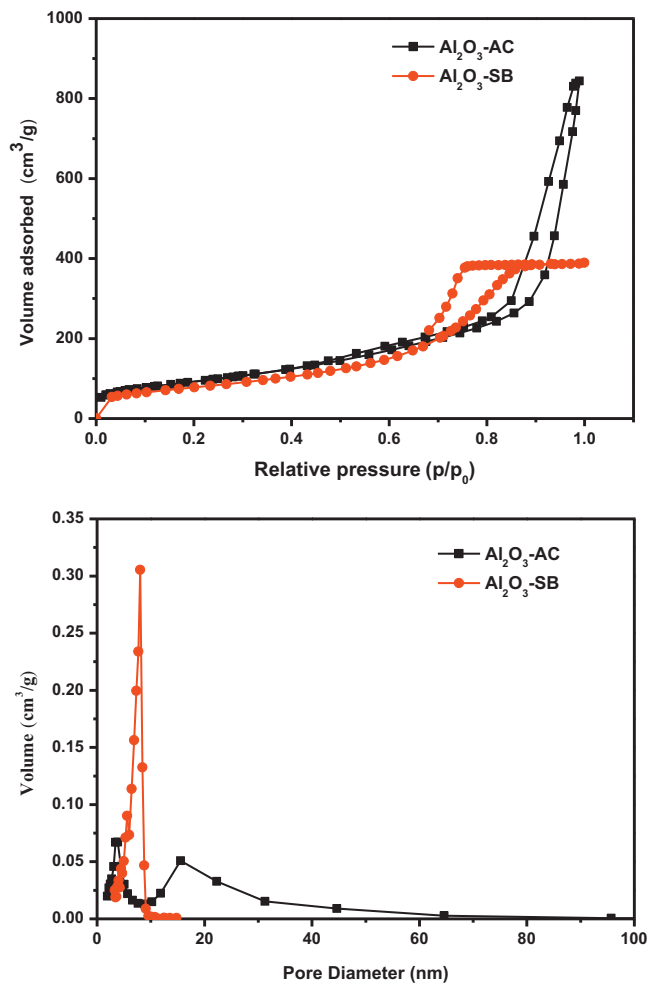


Fig. 3. The pore size distribution profiles and nitrogen adsorption–desorption isotherms of Al_2O_3 -AC and Al_2O_3 -SB.

Al_2O_3 -SB, evidencing the larger pore volume of Al_2O_3 -AC. According to the pore size distributions, Al_2O_3 -AC is featured with the bimodal porous structure, where the smaller pores are narrowly distributed in 2–8 nm and the larger ones exhibit a broad distribution (10–60 nm), while Al_2O_3 -SB has a fairly uniform pore size distribution in the range of 3–10 nm. The morphology of Al_2O_3 -SB with spherical particles can be maintained when it transforms into alumina during thermal transformation process, which leads to uniform particles and centered pore size distribution. In contrast, Al_2O_3 -AC has the morphology of nanorods, leading to stacking mode of particles distinct from that of Al_2O_3 -SB. Therefore, there is a close relationship between pore size distribution of supports and morphology of precursors. Besides, in the process of calcination, NH_3 and CO_2 were released due to the decomposition of Al_2O_3 -AC, which may contribute to a bimodal pore size distribution of alumina. During HDS reaction process, the bimodal pore structure may be beneficial to the reaction performance because the larger pores can enhance the diffusion of reactants and the smaller one can provide the active sites [3].

3.4. Surface property of supports

Fig. 4 shows the ²⁷Al MAS NMR spectra of Al_2O_3 -AC and Al_2O_3 -SB samples. The coordination of surface atoms can be explored by alumina NMR test. As shown in **Fig. 4** for Al_2O_3 -SB, the aluminum species of $\gamma\text{-Al}_2\text{O}_3$ mainly exist in the form of four-fold (AlO_4) and six-fold (AlO_6) coordination, with the resonance peak at 63 ppm

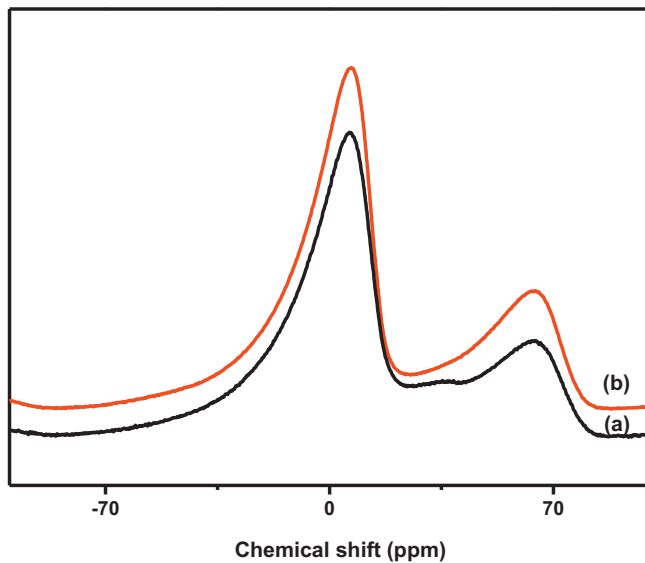


Fig. 4. ²⁷Al MAS NMR patterns of (a) Al_2O_3 -AC and (b) Al_2O_3 -SB.

and 0 ppm, respectively. In contrast, except peaks at 63 ppm and 0 ppm, resonance peak at 34 ppm occurs in the ²⁷Al MAS NMR spectra of Al_2O_3 -AC, which should be assigned to five-fold coordinated aluminum (AlO_5). According to the results in the reference [26], the five-fold coordinated aluminum species are mainly located at (100) crystallographic surfaces in $\gamma\text{-Al}_2\text{O}_3$, and their content is related to the exposure proportion of (100) surfaces.

3.5. Crystalline structure of catalysts

Fig. 5 shows the XRD patterns of oxidic and sulfided NiMo/ Al_2O_3 -AC and NiMo/ Al_2O_3 -SB. For oxidic catalysts, very broad diffraction peaks of $\gamma\text{-Al}_2\text{O}_3$ are observed. However, there is no XRD evidence for the presence of crystalline MoO_3 and NiO phases, suggesting that such phases, if present, have crystal sizes smaller than 4 nm [3,27]. As to sulfided catalysts, similar peaks ascribed to $\gamma\text{-Al}_2\text{O}_3$ are also found, and very weak signals of MoS_2

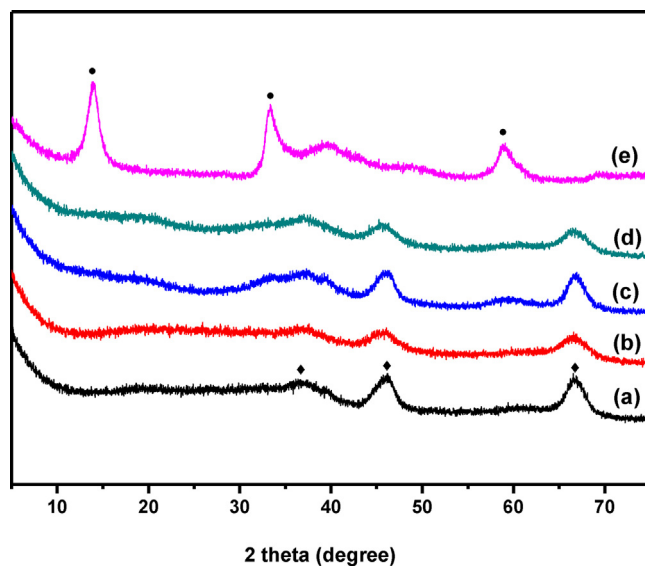


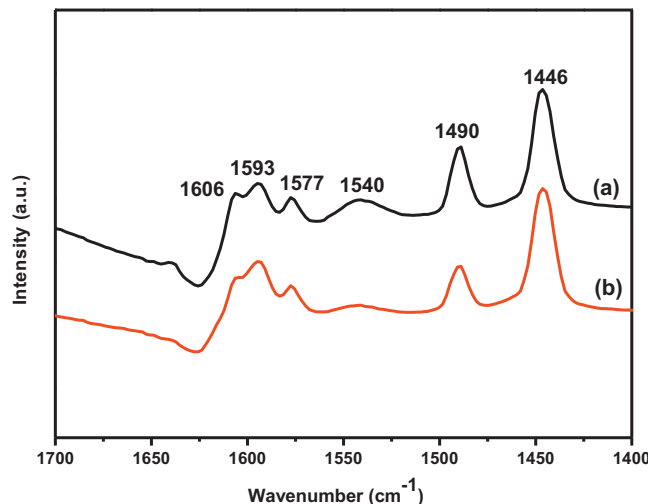
Fig. 5. XRD patterns of fresh and sulfided catalysts (a) $\text{NiMo}/\text{Al}_2\text{O}_3$ -AC; (b) $\text{NiMo}/\text{Al}_2\text{O}_3$ -SB; (c) sulfided $\text{NiMo}/\text{Al}_2\text{O}_3$ -AC; (d) sulfided $\text{NiMo}/\text{Al}_2\text{O}_3$ -SB; (e) MoS_2 (● – MoS_2 ; ◆ – $\gamma\text{-Al}_2\text{O}_3$).

Table 3

Product distributions of HDS reaction of DBT.

Catalysts	CHB (%m)	BP (%m)	DBT (%m)	DBT conversion ^a (%m)	CHB selectivity ^b
NiMo/Al ₂ O ₃ -SB	7.11	59.86	33.03	66.97	0.12
NiMo/Al ₂ O ₃ -AC	11.19	68.39	20.42	79.58	0.16

CHB: cyclohexylbenzene; BP: biphenyl; DBT: dibenzothiophene.

^a DBT conversion % = wt_(BP+CHB)/total amount of DBT.^b CHB selectivity = wt_{CHB}/wt_{BP}.**Fig. 6.** IR spectra of pyridine adsorbed on (a) NiMo/Al₂O₃-AC and (b) NiMo/Al₂O₃-SB catalysts.

diffraction peaks at $2\theta = 33.1^\circ$ and 58.5° are identified only in sulfided NiMo/Al₂O₃-AC, indicating a little difference in the MoS₂ particle size over these two catalysts. Therefore, MoS₂ particles are almost uniformly dispersed on the surface of both Al₂O₃-AC and Al₂O₃-SB, and the differences in MoS₂ particle size may affect the catalytic performance [28,29].

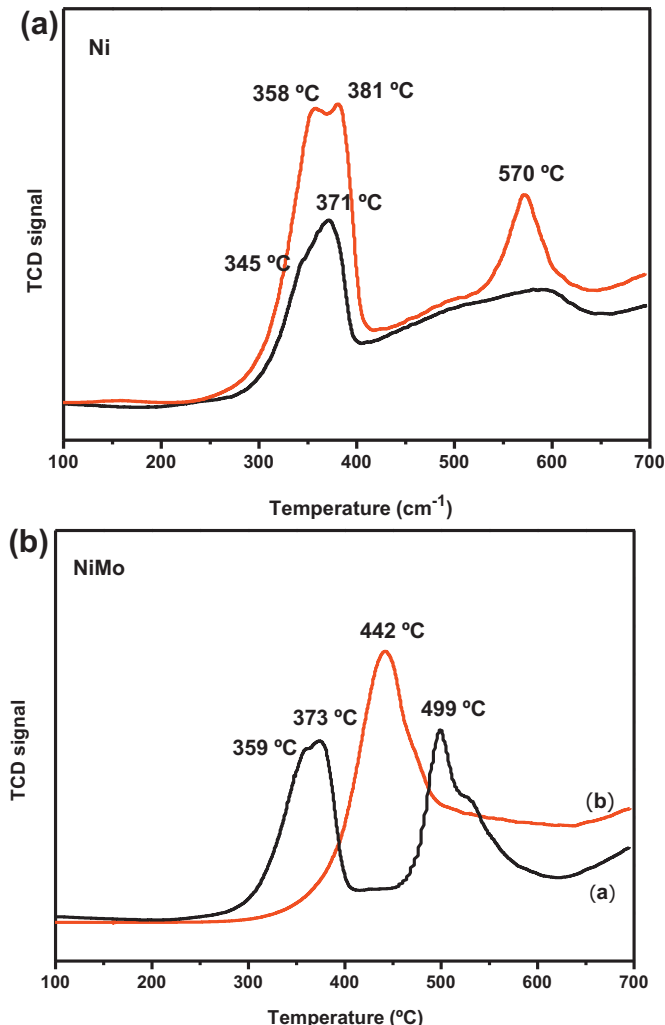
3.6. Acid property of catalysts

Fig. 6 shows the IR spectra of pyridine adsorption of NiMo/Al₂O₃ catalysts. It can be seen from Fig. 6 that NiMo/Al₂O₃-AC and NiMo/Al₂O₃-SB show similar bands in the region 1700–1400 cm⁻¹. The band at 1540 cm⁻¹, 1490 cm⁻¹ and 1450 cm⁻¹ are associated with pyridine adsorbed on Brønsted acid sites, pyridine adsorbed on both Brønsted and Lewis acid sites, and pyridine adsorbed on Lewis acid sites [30], respectively. Besides, the band intensity of NiMo/Al₂O₃-AC at 1450 cm⁻¹ is almost the same as that of NiMo/Al₂O₃-SB while the bands of NiMo/Al₂O₃-AC at 1540 cm⁻¹ and 1490 cm⁻¹ are more intensive than those of NiMo/Al₂O₃-SB, indicating higher Brønsted acid sites concentration of NiMo/Al₂O₃-AC [31].

The NH₃-TPD data of the oxidic catalysts are also listed in Table 1. The total acidity is increased by the impregnation of molybdenum and nickel ions. Furthermore, NiMo/Al₂O₃-AC contains more weak and medium strong acid sites than NiMo/Al₂O₃-SB, which may be related to the content of Brønsted acid sites [32]. Duan et al. [33] reported that HDS activity could be enhanced by higher Brønsted acid sites concentration, which is consistent with the results of our following HDS test.

3.7. Temperature-programmed reduction (TPR) for catalysts

Fig. 7 represents the TPR patterns of Ni and NiMo supported on Al₂O₃-AC and Al₂O₃-SB. For Ni/Al₂O₃-AC, the TPR pattern exhibits

**Fig. 7.** TPR patterns of Ni and NiMo supported on (a) Al₂O₃-AC and (b) Al₂O₃-SB.

three reduction peaks in the 200–700 °C region. The first peak centered at 345 °C may be related to the reduction of NiO to Ni⁰, and the second reduction peak at 371 °C may be due to the interaction of Ni²⁺ species with alumina [34]. According to the reference [35], the third peak at 570 °C can be attributed to the reduction of nickel–aluminum species. In contrast, for Ni/Al₂O₃-SB, the first and second reduction peaks are about 10 °C higher than those of Ni/Al₂O₃-AC, indicating that Ni²⁺ species have relatively strong interaction with alumina and are more difficult to be reduced than Ni²⁺ supported on Al₂O₃-AC. Furthermore, the third reduction peak of Ni/Al₂O₃-AC at 570 °C is less intensive than that of Ni/Al₂O₃-SB, evidencing that the metal dispersion of Ni/Al₂O₃-AC is superior to that of Ni/Al₂O₃-SB. Therefore, Al₂O₃-AC may promote the formation of NiMoS active phase, which would lead to the enhancement of catalytic activity over NiMo catalysts.

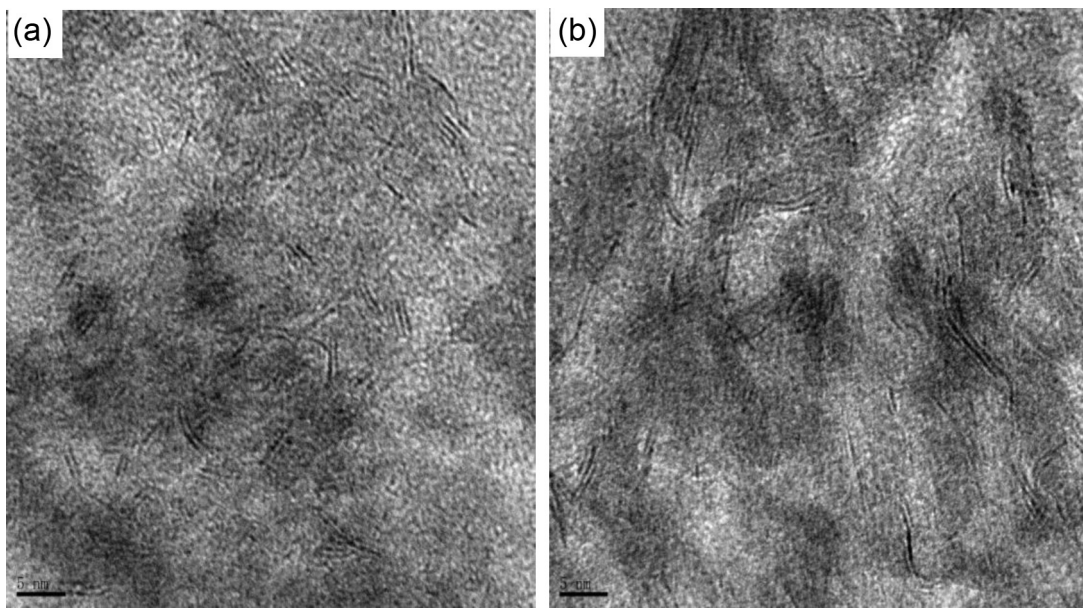


Fig. 8. HRTEM micrographs of sulfided (a) NiMo/Al₂O₃-AC and (b) NiMo/Al₂O₃-SB catalysts.

It appears three reduction peaks in the TPR profile recorded on the NiMo/Al₂O₃-AC. The first peak at about 359 °C and the second peak at about 373 °C are related to the reduction of Ni species and partial reduction of octahedrally coordinated polymeric Mo species. The third peak at about 499 °C is attributed to the further reduction of polymolybdate, which exerts stronger interaction with the support. In the case of NiMo/Al₂O₃-SB, the reduction peak of Ni and Mo oxides occurs at about 442 °C and further reduction of polymolybdate is not observed until 700 °C, indicating that NiMo/Al₂O₃-SB exhibits stronger metal-support interaction. It is generally known that the catalyst pre-sulfurization operation would be difficult if Ni and Mo species have strong interaction with alumina support, which may lead to poor catalytic performance of HDS. Therefore, the TPR results reveal that the active species of NiMo/Al₂O₃-AC are more easily sulfided than those of NiMo/Al₂O₃-SB, indicating that Al₂O₃-AC favors the sulfurization of active metal [36,37], which can be well verified in the following HDS activity test.

3.8. HDS activity

Product distributions of the HDS reaction of DBT over those two catalysts are listed in Table 3. As seen from Table 3, the conversion of DBT for NiMo/Al₂O₃-AC is 12.61% higher than that for NiMo/Al₂O₃-SB. Besides, the CHB/BP values of those two catalysts are less than 1, indicating that the direct hydrogenolysis (DDS) reaction occurs faster than the hydrogenation (HYD) reaction.

Fig. 8 shows the HRTEM images of sulfided NiMo/Al₂O₃-AC and NiMo/Al₂O₃-SB. It can be seen that the dispersion of visible MoS₂ particles on the surface of Al₂O₃-AC is better than that of Al₂O₃-SB. Fig. 9 shows the length and layer stacking distributions of MoS₂ crystallites in sulfided NiMo catalysts supported on Al₂O₃-AC and Al₂O₃-SB. In Fig. 9, the number of layer stacking of MoS₂ particles of NiMo/Al₂O₃-AC is in the range of 1–3 with two layer stacking accounting for 50%, while NiMo/Al₂O₃-SB has single layer which occupies 75%. Besides, the length of MoS₂ particles of NiMo/Al₂O₃-SB is longer than that of NiMo/Al₂O₃-AC. According to relevant references [38–40], there are two types of Ni-Mo-S active phases: single layer (type I) and multilayer (type II). Specifically, type I has stronger interaction with alumina support while type II has weaker interaction with alumina support. Furthermore, the desulfurization activity of type II almost doubles that of type I and the

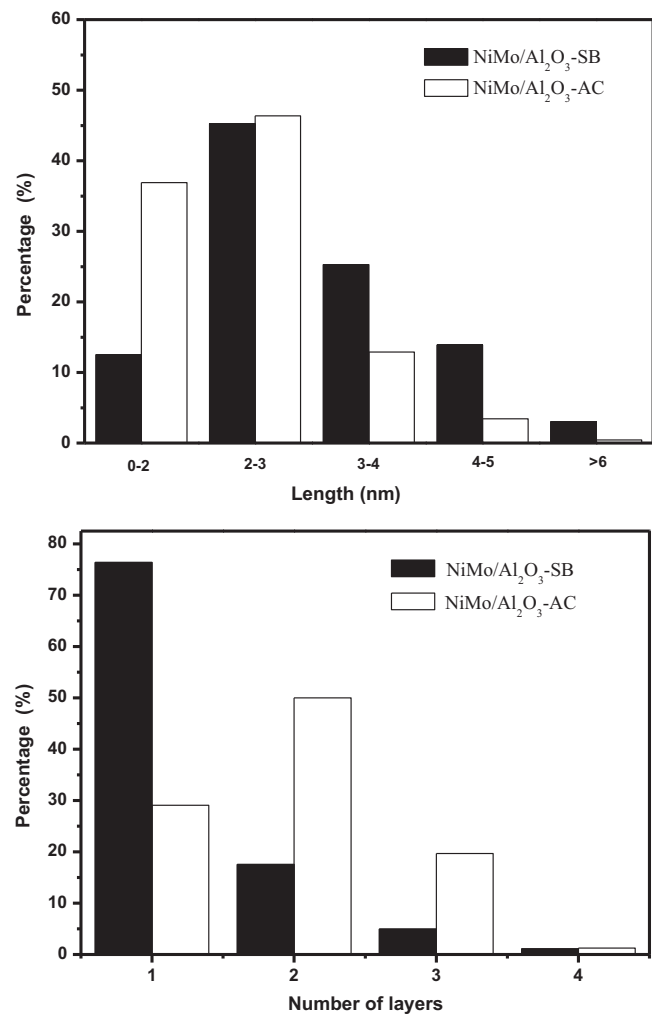


Fig. 9. Length and layer stacking distributions of MoS₂ crystallites in sulfided NiMo catalysts supported on Al₂O₃-AC and Al₂O₃-SB.

type of active phase has close relationship with the surface properties of alumina support. Combined with Fig. 9, it reveals that the active phase of NiMo/Al₂O₃-AC mainly exists as type II while the active phase of NiMo/Al₂O₃-SB mainly exists as type I. Therefore, the results of HRTEM and MoS₂ stacking layers distribution are in good agreement with TPR results and the HDS performance of NiMo catalysts.

4. Conclusion

In conclusion, the precursor AACH consisted of uniform nanorods was successfully prepared by a solid-state reaction, then Al₂O₃-AC was obtained after the calcination of AACH. Compared to Al₂O₃-SB prepared by the calcination of commercial SB, Al₂O₃-AC had higher specific surface area, larger pore volume, unique bimodal porous structure, and more weak and moderate Lewis acid sites. Interestingly, Al₂O₃-AC had five-fold coordinated aluminum (AlO₅) on the surface while Al₂O₃-SB only had four-fold (AlO₄) and six-fold coordinated aluminum (AlO₆). Furthermore, XRD patterns showed that active components of NiMo/Al₂O₃-AC supported on Al₂O₃-AC were uniformly dispersed. Remarkably, NiMo/Al₂O₃-AC exhibited more Brønsted acid sites and weaker metal-support interaction than NiMo/Al₂O₃-SB supported on Al₂O₃-SB. Therefore, catalytic evaluation results showed that NiMo/Al₂O₃-AC had higher conversion ratio of DBT for HDS reaction than NiMo/Al₂O₃-SB.

Acknowledgment

Financial support from “the Fundamental Research Funds for the Central Universities” 13CX06052A is gratefully acknowledged.

References

- [1] Y. Okamoto, M. Breysse, G.M. Dhar, C. Song, *Catal. Today* 86 (2003) 1–4.
- [2] J.P.R. Vissers, B. Scheffer, V.H.J. de Beer, J.A. Moulijin, R. Prins, *J. Catal.* 105 (1987) 277–284.
- [3] X.M. Liu, X. Li, Z.F. Yan, *Appl. Catal., B: Environ.* 121–122 (2012) 50–56.
- [4] M. Breysse, P. Afanasiev, C. Geantet, M. Vrinat, *Catal. Today* 86 (2003) 5–16.
- [5] L. Ji, J. Lin, K.L. Tan, H.C. Zeng, *Chem. Mater.* 12 (2000) 931–939.
- [6] K. Hellgardt, D. Chadwick, *Ind. Eng. Chem. Res.* 37 (1998) 405–411.
- [7] Z. Zhang, T.J. Pinnavaia, *J. Am. Chem. Soc.* 124 (2002) 12294–12301.
- [8] W.Q. Cai, Y.Z. Hu, J. Chen, G.X. Zhang, T. Xia, *CrystEngComm* 14 (2012) 972–977.
- [9] Z.R. Zhang, T.J. Pinnavaia, *Langmuir* 26 (2010) 10063–10067.
- [10] G.C. Li, Y.Q. Liu, D. Liu, L.H. Liu, C.G. Liu, *Mater. Res. Bull.* 45 (2010) 1487–1491.
- [11] S.J. Wilson, *J. Solid State Chem.* 30 (1979) 247–255.
- [12] G.C. Li, Y.Q. Liu, L.L. Guan, X.F. Hu, C.G. Liu, *Mater. Res. Bull.* 47 (2012) 1073–1079.
- [13] Y.T.O. S.W. Kim, D.C. Shin, *Colloids Surf., A* 313–314 (2008) 415–418.
- [14] W.L. Wang, J.Q. Bi, Y.Q. Qi, Z. Zhang, Z. Xing, H.L. Zhu, D. Guo, J.J. Xu, Y.J. Bai, *Powder Technol.* 201 (2010) 273–276.
- [15] J.G. Li, X.D. Sun, M. Zhang, X.D. Li, H.Q. Ru, J. Inorg. Mater. 13 (1998) 803–807.
- [16] X.F. Hu, Y.Q. Liu, Z. Tang, G.C. Li, R.Y. Zhao, C.G. Liu, *Mater. Res. Bull.* 47 (2012) 4271–4277.
- [17] G.C. Li, Y.Q. Liu, Z. Tang, G.C. Liu, *Appl. Catal., A: Gen.* 437–438 (2012) 79–89.
- [18] E.P. Parry, *J. Catal.* 2 (1963) 371–379.
- [19] G. Busca, *Catal. Today* 41 (1998) 191–206.
- [20] X.S. Liu, R.E. Truitt, *J. Am. Chem. Soc.* 119 (1997) 9856–9860.
- [21] C. Morterra, G. Magnacca, *Catal. Today* 27 (1996) 497–532.
- [22] X.S. Liu, *J. Phys. Chem. C* 112 (2008) 5066–5073.
- [23] J.R. Grzechowiak, J. Rynkowski, I. Wereszczako-Zielinska, *Catal. Today* 65 (2001) 225–231.
- [24] M. Lewandowski, Z. Sarbak, *Fuel* 79 (2000) 487–495.
- [25] U. Usman, M. Takaki, T. Kubota, Y. Okamoto, *Appl. Catal., A: Gen.* 286 (2005) 148–154.
- [26] M. Digne, P. Sautet, P. Raybaud, P. Euzen, H. Toulhoat, *J. Catal.* 226 (2004) 54–68.
- [27] D. Solís, A.L. Agudo, J. Ramírez, T. Klimova, *Catal. Today* 116 (2006) 469–477.
- [28] B. Liu, Y.M. Chai, Y.J. Wang, T.T. Zhang, Y.Q. Liu, G.C. Liu, *Appl. Catal., A: Gen.* 388 (2012) 248–255.
- [29] G. Berhault, M.P.D.I. Rosa, A. Mehta, M.J. Yácaman, R.R. Chianelli, *Appl. Catal., A: Gen.* 345 (2008) 80–88.
- [30] M.E. Cervantes-Gaxiola, M. Arroyo-Albiter, A. Pérez-Larios, P.B. Balbuena, J. Espino-Valencia, *Fuel* 113 (2013) 733–743.
- [31] H. Kim, J.J. Lee, S.H. Moon, *Appl. Catal., B: Environ.* 44 (2003) 287–299.
- [32] D. Ferdous, A.K. Dalai, J. Adjaye, *Appl. Catal., A: Gen.* 260 (2004) 137–151.
- [33] A.J. Duan, G.F. Wan, Z. Zhao, C.M. Xu, Y.Y. Zheng, Y. Zhang, T. Dou, X.J. Bao, K. Chung, *Catal. Today* 119 (2007) 13–18.
- [34] S.B. Ren, J.S. Qiu, C.Y. Wan, B.L. Xu, Y.N. Fan, Y. Chen, *Chin. J. Catal.* 28 (2007) 651–656.
- [35] L.F. Zhang, J.F. Lin, Y. Chen, *J. Chem. Soc., Faraday Trans.* 88 (1992) 497–502.
- [36] A. Dandekar, R.T.K. Baker, M.A. Vannice, *Carbon* 36 (1998) 1821–1831.
- [37] H. Shang, C. Liu, Y. Xu, J. Qiu, F. Wei, *Fuel Process. Technol.* 88 (2007) 117–123.
- [38] M. Daage, R.R. Chianelli, *J. Catal.* 149 (1994) 414–427.
- [39] Y.M. Chai, G.J. An, Y.Q. Liu, C.G. Liu, *Prog. Chem.* 19 (2007) 234–242.
- [40] J. Liu, Y.S. Zhao, Y. Liu, R.Y. Zhao, C.G. Liu, *Acta Petrolei Sin.* 26 (2010) 517–524.